PHILOSOPHICAL TRANSACTIONS OF THE ROYAL SOCIETY A

Phil. Trans. R. Soc. A (2008) **366**, 4061–4075
doi:10.1098/rsta.2008.0101
Published online 30 September 2008

Accretion of the Earth

By Robin M. Canup*

Southwest Research Institute, Planetary Science Directorate, 1050 Walnut Street, Suite 400, Boulder, CO 80302, USA

The origin of the Earth and its Moon has been the focus of an enormous body of research. In this paper I review some of the current models of terrestrial planet accretion, and discuss assumptions common to most works that may require re-examination. Density-wave interactions between growing planets and the gas nebula may help to explain the current near-circular orbits of the Earth and Venus, and may result in large-scale radial migration of proto-planetary embryos. Migration would weaken the link between the present locations of the planets and the original provenance of the material that formed them. Fragmentation can potentially lead to faster accretion and could also damp final planet orbital eccentricities. The Moon-forming impact is believed to be the final major event in the Earth's accretion. Successful simulations of lunar-forming impacts involve a differentiated impactor containing between 0.1 and 0.2 Earth masses, an impact angle near 45° and an impact speed within 10 per cent of the Earth's escape velocity. All successful impacts—with or without pre-impact rotation—imply that the Moon formed primarily from material originating from the impactor rather than from the proto-Earth. This must ultimately be reconciled with compositional similarities between the Earth and the Moon.

Keywords: accretion; planet formation; origin of the Earth; origin of the Moon

1. Dynamics of terrestrial accretion

Solid planets are believed to form through the process of accretion, in which collisions between Sun-orbiting objects lead to growth of progressively larger bodies. It is envisioned that planetary accretion began within a circumsolar disc of gas (primarily hydrogen) and dust produced as a by-product of the collapse of a molecular cloud core to form the Sun. Observations of young stars suggest that the Sun's gaseous nebula dispersed on a time scale $\tau_{\rm neb}$ of 10^6 to 10^7 years (e.g. Haisch *et al.* 2001). Isotopic studies indicate that the Earth's accretion was more protracted, ending at approximately 50 Myr (e.g. Halliday & Kleine 2006).

(*a*) *Processes*

A common initial condition used by planet formation models is the minimum mass solar nebula (MMSN), constructed by spreading into a disc the mass contained in the current planets, augmented to bulk solar composition. In the

*robin@boulder.swri.edu

One contribution of 14 to a Discussion Meeting Issue 'Origin and differentiation of the Earth: past to present'.

terrestrial planet region, an MMSN disc has a solid surface density $\sigma_{\mathrm{S,\,MMSN}} = \sigma_{\mathrm{S,1\,AU}}(1\,\mathrm{AU}/a)^{\alpha}$ at semi-major axis a, with $\sigma_{\mathrm{S,1\,AU}} \approx 7\,\mathrm{g\,cm^{-2}}$ and $\alpha = 3/2$, and a gas surface density $\sigma_{\mathrm{G,\,MMSN}} = f\sigma_{\mathrm{S,\,MMSN}}$, where $f \sim 240$ is the solar gas-to-solids ratio in the inner Solar System (Hayashi *et al.* 1985).

The processes responsible for the earliest stages of planetesimal growth from dust particles to kilometre-sized objects are actively debated. Small particles are strongly affected by interactions with the gas, which cause their mutual collision velocities to greatly exceed their escape velocities, precluding gravity-based accretion. Two proposed solutions invoke either non-gravitational sticking forces (e.g. Weidenschilling & Cuzzi 1993) or concentration of solids until gravitational instability causes direct collapse into larger objects (e.g. Ward 2000; Johansen *et al.* 2007).

Once kilometre-sized 'planetesimals' are formed, their growth rate is controlled by their collision rate, itself a function of the planetesimal masses and dispersion velocities v_{ran}. The mass accretion rate of a planetesimal of radius R and mass M due to collisions with smaller objects having a surface density σ_{S} is $\dot{M} \sim \pi R^2 \sigma_{\mathrm{S}} \Omega [1 + (v_{\mathrm{esc}}/v_{\mathrm{ran}})^2]$, where $\Omega = \sqrt{GM_{\odot}/r^3}$ is the orbital frequency at radius r and $M_{\odot}$ is the solar mass. The bracketed factor is the enhancement in the collisional cross-section due to gravitational focusing f_{g}, where $v_{\mathrm{esc}} \equiv 2R\sqrt{2\pi\rho G/3}$ is the planetesimal's escape velocity and ρ is its material density. The accretion time scale (or, alternatively, the time spent as a mass M object) is $\tau_{\mathrm{acc}} \equiv M/\dot{M} \sim (\Omega f_{\mathrm{g}})^{-1}(\rho R/\sigma_{\mathrm{S}})$. Two limiting growth regimes occur: for $v_{\mathrm{ran}} \geq v_{\mathrm{esc}}$, focusing is unimportant ($f_{\mathrm{g}} \sim$ unity) and $\tau_{\mathrm{acc}} \sim \Omega^{-1}(\rho R/\sigma_{\mathrm{S}})$; while for $v_{\mathrm{ran}} \ll v_{\mathrm{esc}}$, $f_{\mathrm{g}} \gg 1$ and $\tau_{\mathrm{acc}} \sim \Omega^{-1} v_{\mathrm{ran}}^2/(8G\sigma_{\mathrm{S}}R)$. In the former, the relative radii of growing objects converge with time because $\tau_{\mathrm{acc}} \propto R$ and growth is 'orderly'; while in the latter mode, $\tau_{\mathrm{acc}} \propto 1/R$, and so the larger objects get, the faster they grow, causing their relative radii to diverge and 'runaway' growth.

Relative velocities are generally increased by gravitational scattering and damped by collisions. The balance of these two processes causes the characteristic dispersion velocity to be comparable to v_{esc} for the size of object containing most of the swarm's mass. In addition, dynamical friction between objects of different sizes damps the velocities of the large objects and excites the velocities of the small objects. A distribution of equal-sized particles will have $v_{\mathrm{ran}} \sim v_{\mathrm{esc}}$ and so initial growth is slow and orderly, but with time some larger particles form. For a surface density of large particles that is much smaller than the small particle surface density, the small body population causes v_{ran} to be much smaller than the escape velocity of the largest objects, so that the larger objects grow in the runaway regime. Near 1 AU in an MMSN disc, runaway growth allows kilometre-sized planetesimals to accrete into $10^{-3}M_{\oplus}$ planetary embryos in only about 10^4 years (e.g. Kenyon & Bromley 2006).

Ultimately, runaway growth is self-limiting. As an increasing fraction of the total mass is contained in large objects, the supply of small bodies that can be accreted is diminished. Viscous stirring by the large objects begins to dominate over that of the small bodies (e.g. Goldreich *et al.* 2004), and dynamical friction by the reduced small particle population is weakened, leading to increased dispersion velocities. An increasing v_{ran} and a decreasing σ_{S} cause the growth of the large objects to slow to an orderly rate in which their relative sizes converge with time. This 'oligarchic' growth stage (e.g. Thommes *et al.* 2003) is typified by a system of

similarly sized large embryos that each dominates their own accretional annulus within the disc. In the limit that an oligarch accretes all of its annulus' material, its mass is the isolation mass, $M_{\rm iso} \equiv 2\pi a \Delta a \sigma_{\rm S}$. For an annulus width Δa that scales with the mutual Hill radius of neighbouring oligarchs so that $\Delta a = ba(2M_{\rm iso}/3M_{\odot})^{1/3}$ (i.e. shear-dominated oligarchy; Goldreich *et al.* 2004),

$$M_{\rm iso} \sim 0.09 M_{\oplus} \left(\frac{b}{10}\right)^{3/2} \left(\frac{\sigma_{\rm S,\,1\ AU}}{7\ {\rm g\ cm^{-2}}}\right)^{3/2} \left(\frac{a}{1\ {\rm AU}}\right)^{3-3\alpha/2}, \tag{1.1}$$

and the time to form such an object (assuming that small objects are stirred by the oligarchs and damped by aerodynamic gas drag) is (Kokubo & Ida 2002)

$$t_{\rm iso} \sim 0.4 \times 10^{6}\ {\rm year} \left(\frac{7\ {\rm g\ cm^{-2}}}{\sigma_{\rm S,\,1\ AU}}\right)^{9/10} \left(\frac{a}{1\ {\rm AU}}\right)^{(9\alpha+16)/10} \left(\frac{b}{10}\right)^{1/10}. \tag{1.2}$$

For an MMSN disc, lunar-to-Mars mass oligarchs (0.01–$0.1 M_{\oplus}$) accrete in the terrestrial region on time scales shorter than the expected nebular lifetimes, and a disc containing a greater solid mass than the MMSN would produce more massive oligarchs on still shorter time scales.

Once terrestrial objects achieve masses greater than or about $10^{-2} M_{\oplus}$, their density-wave interactions with the gas nebula become important, depending on the amount of gas still present at that time. The gravitational interactions between an embryo and the spiral density waves it induces in an accompanying gas disc damp the embryo's orbital eccentricity and inclination (e.g. Ward 1998) and cause a secular decay of its semi-major axis a, through an effect known as type I migration (Ward 1986). Both effects become more important as an embryo grows. The type I migration time scale $\tau_1 \equiv a/\dot{a}$ for a mass $M_{\rm P}$ embryo is

$$\tau_1 \sim \frac{1}{C_a \Omega} \left(\frac{M_{\odot}}{M_{\rm P}}\right) \left(\frac{M_{\odot}}{r^2 \sigma_{\rm G}}\right) \left(\frac{c}{r\Omega}\right)^2, \tag{1.3}$$

where C_a is a constant, approximately 4.4 for an MMSN disc (Tanaka *et al.* 2002); $\sigma_{\rm G}$ is the gas surface density; and $(c/r\Omega)$ is the disc aspect ratio. The time scale for density-wave damping to circularize an orbit is shorter, with $\tau_{\rm ecc} \sim (c/r\Omega)^2 \tau_1$ and $(c/r\Omega) \sim 0.05 (a/1\ {\rm AU})^{\beta}$ with $\beta = 1/4$ commonly invoked.

Eventually the system of oligarchs destabilizes, their mutual interactions drive their dispersion velocities to values comparable with their escape velocities, and the system enters a chaotic final stage lasting for approximately 10^7–10^8 years and dominated by mutual oligarch collisions. For a gas-free disc, this transition occurs when the oligarchs contain roughly half of the total solid surface density (Goldreich *et al.* 2004), which occurs after approximately 10^6 years for an MMSN disc and at earlier times for more massive discs (Kenyon & Bromley 2006). If a portion of the gas nebula remains at this time, destabilization of the oligarchs and the onset of the large impact phase may be delayed by density-wave damping until $\sigma_{\rm G} < \sigma_{\rm S}$ (Goldreich *et al.* 2004).

(*b*) *Example simulations*

Numerical simulations of the accretion of planetesimals into planets often rely upon a hybrid approach (e.g. Weidenschilling *et al.* 1997; Kenyon & Bromley 2006), in which a statistical treatment of small particles is combined with a

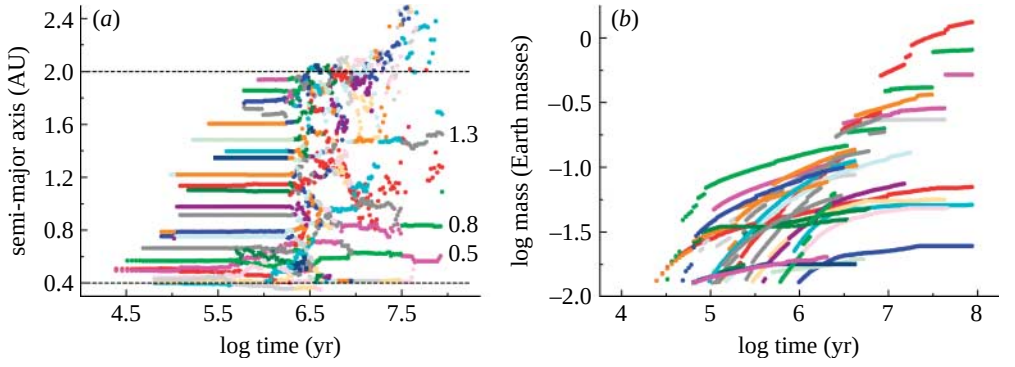

Figure 1. The time evolution of planetary embryos with $M_P > 10^{-2} M_\oplus$ from a Kenyon & Bromley (2006) hybrid accretion simulation whose initial disc contained $\sigma_{S,\,1\,AU} = 8\,g\,cm^{-2}$ in 5 km planetesimals. (*a*) The evolution of semi-major axis with time, with the numbers at 10^8 years indicating masses in $M_\oplus$ of the three large final planets; (*b*) $M_P(t)$ for the same objects, where discrete jumps indicate large accretionary events. In both (*a*,*b*), a given colour track ends when an object collides with a larger embryo. Runaway growth leads to lunar-sized embryos in 3×10^4 to 5×10^5 years between 0.4 and 2 AU, respectively. Moving from the inner to the outer disc, the onset of chaos and oligarch–oligarch collisions occurs at approximately 4×10^5 to 3×10^6 years. More massive initial discs evolve into the chaotic phase at earlier times (Kenyon & Bromley 2006).

discrete treatment for the large objects. Figure 1 shows the time evolution of oligarchs in a Kenyon & Bromley (2006) simulation that begins with 5 km planetesimals, assumes that collisions result in mergers, and evolves bodies with direct *N*-body simulation once their masses exceed approximately $10^{-2} M_\oplus$. Runaway growth leads to the first object achieving this mass in only about 10^4 years. The chaotic growth stage is clearly seen in figure 1*a* as the oligarchs perturb one another into crossing orbits. After 10^8 years, three planets between 0.4 and 2 AU each contain more than $0.5 M_\oplus$, while three others are less than $0.07 M_\oplus$ (figure 1*b*).

Alternatively, a pure *N*-body approach can be used to model the final stage of oligarch accretion into planets. The first such models (Chambers & Wetherill 1998; Agnor *et al.* 1999; Chambers 2001) considered approximately 20–150 initial embryos and assumed a gas-free disc. Recently, Kokubo *et al.* (2006) performed approximately 200 similar calculations, whose results were generally consistent with those of the earlier works. An initial MMSN disc between 0.5 and 1.5 AU accretes into 2 ± 0.6 major planets, with the two largest having masses $1.27\pm0.25 M_\oplus$ and $0.66\pm0.23 M_\oplus$, and semi-major axes 0.75 ± 0.20 AU and 1.12 ± 0.53 AU (Kokubo *et al.* 2006), roughly comparable to those of the Earth and Venus ($0.8 M_\oplus$ and $a = 0.72$ AU). However, the simulated planets have eccentricities and inclinations that are typically much higher than those of the Earth and Venus. Two effects not included in most *N*-body simulations could result in more circular final planet orbits: dynamical friction with background planetesimals (e.g. Chambers & Wetherill 1998) and/or the density-wave damping with a remnant of solar nebula having $\sigma_G \sim 10^{-4}$–$10^{-3} \sigma_{G,\,MMSN}$ (Agnor & Ward 2000). Both solutions to the 'high-eccentricity problem' appear promising. *N*-body simulations that consider an initial system with half its total mass in approximately $0.1 M_\oplus$ embryos and half in approximately $10^{-3} M_\oplus$ planetesimals yield some systems

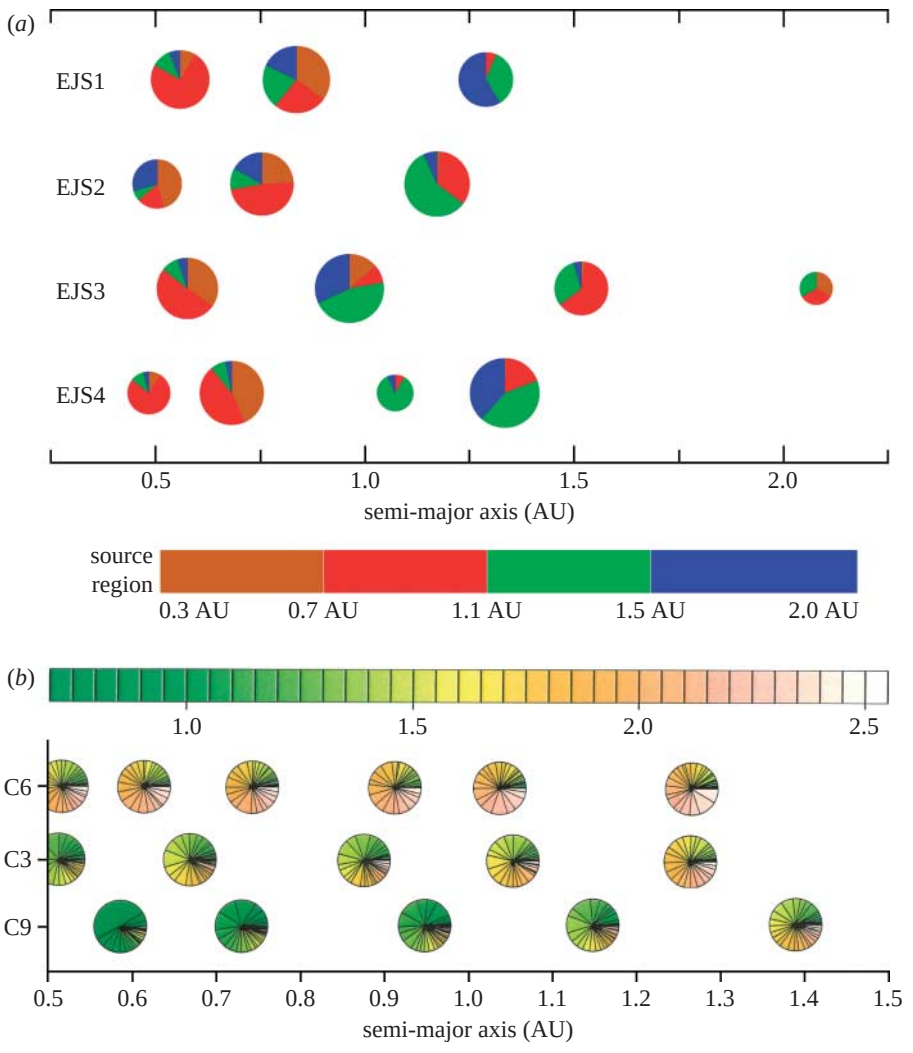

Figure 2. Composition of final planets from simulations by (*a*) O'Brien *et al.* (2006, with diameters proportional to the planet diameter) and (*b*) McNeil *et al.* (2005). Colour bars indicate the original radial location in AU of each mass component. The O'Brien *et al.* simulations are the highest-resolution *N*-body models performed to date; those shown in (*a*) consider an initial disc with $\sigma_{\mathrm{S},1\ \mathrm{AU}}=8\ \mathrm{g\ cm^{-2}}$, include Jupiter and Saturn with their present eccentric orbits, and find substantial radial mixing of material inside 2 AU. The McNeil *et al.* simulations in (*b*) consider a more massive initial disc with $\sigma_{\mathrm{S},1\ \mathrm{AU}}=21\ \mathrm{g\ cm^{-2}}$, and include type I migration with $C_a=3.1$ and $\{c/r\Omega\}_{1\ \mathrm{AU}}=0.07$ (see equation (1.3)) by a gas nebula with an exponential decay time scale of $\tau_{\mathrm{neb}}=0.5$ (run C9), 1 (run C3) and 2 (run C6) Myr. Longer τ_{neb} leads to more migration and loss to collision with the Sun. While each case initially had approximately $5M_{\oplus}$ of solid material in the 0.5–1.5 AU region, the final mass in this region is $2.9M_{\oplus}$, $2.6M_{\oplus}$ and $1.7M_{\oplus}$ for runs C9, C3 and C6, respectively. In the case with the most migration (C6), final embryos near 1 AU are composed primarily of material that originated outside 2 AU.

whose angular momentum deficits (a measure of how dynamically excited a system is compared to one with circular, coplanar orbits) are comparable to that of the current inner Solar System, which has been attributed to more effective dynamical

friction (O'Brien *et al.* 2006). Nagasawa *et al.* (2005) considered isolation mass objects distributed from 0.5 to 3 AU subject to density-wave damping, and tracked the system as the solar nebula depletes and the secular resonance associated with Jupiter's orbital apsidal precession (ν_5) 'sweeps' through the terrestrial planet region. Their simulations produced final terrestrial systems with appropriate masses and eccentricities if the nebula depletion time scale exceeds 3 Myr (Nagasawa *et al.* 2005).

(*c*) *Implications*

During late stage accretion, large impacts occur with random orientation and yield rapid planetary spin rates (Agnor *et al.* 1999). The last large impacts onto Earth-sized planets occur at an average time of 25–50 Myr depending on model specifics (Agnor *et al.* 1999; Nagasawa *et al.* 2005; O'Brien *et al.* 2006). Median times for the Earth analogues to reach 50 per cent (90 per cent) of their final mass are 10–20 (40–50) Myr (Chambers 2001; O'Brien *et al.* 2006). Such values are in reasonable agreement with the age of the Earth inferred from isotopic systems (e.g. Halliday & Kleine 2006).

Substantial radial mixing of disc material is expected during final planet assembly. Figure 2 shows the provenance of material that comprises the final planets in example simulations. For their final planets, O'Brien *et al.* (2006) derived a mass-weighted median value $\delta a \sim 0.5a$, where δa is the difference between an embryo's initial semi-major axis and that of the final planet into which it is accreted. This implies that a planet at 1 AU on average comprises material originally located between 0.5 and 1.5 AU. Figure 2*a* also reflects a stochastic element to the final compositions: they do not always vary predictably with semi-major axis (e.g. the innermost planet in run EJS2 contains the largest fraction of outer disc material), nor do planets at similar final radii in different simulations have the same composition. A key implication is that the Moon-forming impactor is unlikely to have had an identical composition to the proto-Earth.

(*d*) *Open issues*

In the past decade, a relative consensus has developed concerning many of the basic traits of post-planetesimal growth, with a variety of methods predicting similar accretion stages (runaway growth → oligarchic growth → chaotic growth), growth time scales and final planetary system properties. However, these commonalities may be in part due to the similar initial conditions and assumptions made by most models. For example, nearly all simulations neglect fragmentation. During oligarchic growth, stirring by the oligarchs causes collisions between small planetesimals to occur at velocities that greatly exceed their escape velocities, so that substantial fragmentation is expected. As fragmentation produces larger numbers of small particles, collisional damping and gas drag become increasingly effective and can lead to faster overall growth rates (e.g. Goldreich *et al.* 2004). However, it is possible that the formation of gaps in the small particle population by the growing embryos might frustrate or preclude such effects (e.g. Rafikov 2001).

Another pervasive assumption is the starting condition of an MMSN disc, which represents the minimum amount of solar-composition material necessary to produce the current planetary masses. A greater total mass in disc solids may

be needed, e.g. recent models for the accretion of Jupiter's core require disc solid surface densities enhanced by factors of at least two to three relative to the MMSN to produce Jupiter in 1–5 Myr (e.g. Hubickyj *et al.* 2005). Similar enhancements could be necessary to produce Uranus and Neptune (e.g. Goldreich *et al.* 2004).

Type I migration has only recently begun to be incorporated into terrestrial accretion models (e.g. McNeil *et al.* 2005). Type I decay is important for objects whose migration time scale τ_1 is comparable to or shorter than the nebular lifetime $\tau_{\rm neb}$. From equation (1.2) we expect isolation mass objects throughout the terrestrial planet region to form in less than 10^6 years in an MMSN disc, and faster in more massive discs. Given the type I time scale in equation (1.3), and setting $\tau_{\rm neb} \geq \tau_1(M_{\rm iso})$ with $M_{\rm iso}$ from equation (1.1), gives an estimated critical nebular lifetime for which migration of isolation mass objects becomes significant,

$$\tau_{\rm neb} \geq 1.8 \times 10^6 \text{ year} \left(\frac{10}{b}\right)^{3/2} \left(\frac{4.4}{C_a}\right) \left(\frac{240}{f}\right) \left(\frac{7 \text{ g cm}^{-2}}{\sigma_{\rm S,\,1\ AU}}\right)^{5/2} \left(\frac{\{c/r\Omega\}_{1\ \rm AU}}{0.05}\right)^2 \times \left(\frac{a}{1\ \rm AU}\right)^{(5\alpha+4\beta-7)/2}, \tag{1.4}$$

where $\{c/r\Omega\}_{1\ \rm AU}$ is the disc aspect ratio at 1 AU and $\sigma_{\rm G,\,1\ AU} = f\sigma_{\rm S,\,1\ AU}$. Median nebular lifetimes of 3 Myr (Haisch *et al.* 2001) imply substantial migration of terrestrial oligarchs in an MMSN disc. Solar-composition discs more massive than the MMSN will experience greater migration, because increasing the disc mass increases the isolation mass (with $M_{\rm iso} \propto \sigma_{\rm S}^{3/2}$) and the background gas surface density, with both acting to hasten type I decay, with $\tau_1^{-1}(M_{\rm iso}) \propto \sigma_{\rm G} M_{\rm iso} \propto f\sigma_{\rm S}^{5/2}$. For example, migration of oligarchs in a solar-composition disc with $\sigma_{\rm S} = 3\sigma_{\rm MMSN}$ would be substantial for $\tau_{\rm neb} \geq 10^5$ years.

It is possible that type I migration was much less effective than nominal rates imply (e.g. Paardekooper & Mellema 2006). Alternatively, the loss of objects due to migration could have been offset by a larger initial mass reservoir, allowing objects originally outside the terrestrial region to migrate inwards and be 'saved' as the nebula dissipates (McNeil *et al.* 2005). Inward migration would imply that a substantial fraction of the final terrestrial planets originated in the asteroid belt region (figure 2*b*), a cosmochemically important implication that merits further consideration.

2. The Moon-forming impact

The leading theory for the Moon's origin is that it formed as a result of an impact between a Mars-sized object and the young Earth (Hartmann & Davis 1975; Cameron & Ward 1976). The lunar-forming impact was probably also the last major event in the Earth's accretion: substantial addition of material after the Moon-forming impact would tend to make the Moon too iron rich (Canup 2004*a*), and even if such later accretion was limited to the Earth, it would probably cause the Earth's O-isotope composition to diverge from that of the Moon (e.g. Wiechert *et al.* 2001).

(a) Constraints and methods

A successful lunar-forming impact must account for (i) the current Earth–Moon system's angular momentum, $L_{\rm EM} \equiv 3.5 \times 10^{41}$ g cm^2 s^{-1}, (ii) a proto-lunar disc whose mass and angular momentum are sufficient to produce a Moon of mass $M_{\rm L} = 0.012 M_\oplus$ outside the Earth's Roche limit, and (iii) a bulk lunar mass abundance of elemental iron in the few to 10 per cent range (e.g. Canup 2004*a* and references therein).

The Earth–Moon system's angular momentum has decreased over its history due to solar interactions, but its initial value would have been within a few to 10 per cent of its current value (e.g. Canup 2008). If the target proto-Earth and impactor of mean density ρ were not rotating prior to impact, the angular momentum delivered by an impactor of mass $M_{\rm i} \equiv \gamma M_{\rm T}$ is

$$L_{\rm col} = b' M_{\rm T}^{5/3} f(\gamma) \sqrt{\frac{2G}{(4\pi\rho/3)^{1/3}}} \left(\frac{v_{\rm imp}}{v_{\rm esc}}\right) \approx 1.3 L_{\rm EM} b' \left(\frac{M_{\rm T}}{M_\oplus}\right)^{5/3} \left(\frac{\gamma}{0.1}\right) \left(\frac{v_{\rm imp}}{v_{\rm esc}}\right), \quad (2.1)$$

where $b' \equiv \sin(\xi)$ is the scaled impact parameter; ξ is the angle between the surface normal and the impact trajectory (so that a grazing impact has $b' = 1$ and $\xi = 90°$); $M_{\rm T}$ is the total colliding mass (impactor + target); γ is the impactor-to-total mass ratio, $f(\gamma) \equiv \gamma(1-\gamma)\sqrt{\gamma^{1/3} + (1-\gamma)^{1/3}}$; $(v_{\rm imp}/v_{\rm esc})$ is the ratio of the impact velocity to the mutual escape velocity; and $v_{\rm imp}^2 = v_{\rm esc}^2 + v_\infty^2$, where v_∞ is the relative velocity of the target and impactor at large separation. Thus, the requirement that an impact produces a system with the correct angular momentum (i.e. $L_{\rm col} \sim L_{\rm EM}$) defines a multi-dimensional parameter space in b', γ and $v_{\rm imp}$, within which cases that also give the correct lunar mass and low Fe abundance must be identified. Consideration of pre-impact rotation in the proto-Earth and/or the impactor broadens the potential parameter space further.

Hydrodynamical models of giant impacts have primarily used smooth particle hydrodynamics or SPH (e.g. Benz *et al.* 1989; Canup & Asphaug 2001; Canup 2004*a*, 2008). SPH represents matter by spherically symmetric particles whose individual evolutions due to gravity, pressure forces and shock dissipation are calculated as a function of time. The Lagrangian formulation of SPH is ideally suited to tracking mixed materials (iron versus silicate) and particle histories (e.g. whether the mass in the proto-lunar disc originated from the impactor or the target). Recently, a three-dimensional Eulerian model has also been applied to giant impacts (Wada *et al.* 2006). Advantages of grid-based methods over SPH include the potential for high spatial resolution in the orbiting disc, a superior treatment of shocks and improved estimates of volatile loss after the impact. However, the Wada *et al.* (2006) simulations did not consider mixed materials (so that mantle versus core material are not distinguished), and they are computationally intensive. The single Wada *et al.* (2006) simulation using both an equation-of-state appropriate for rocky materials and a grid large enough to track the orbiting material found a predicted satellite mass similar to that determined using SPH for similar collisions, although further comparisons are clearly warranted.

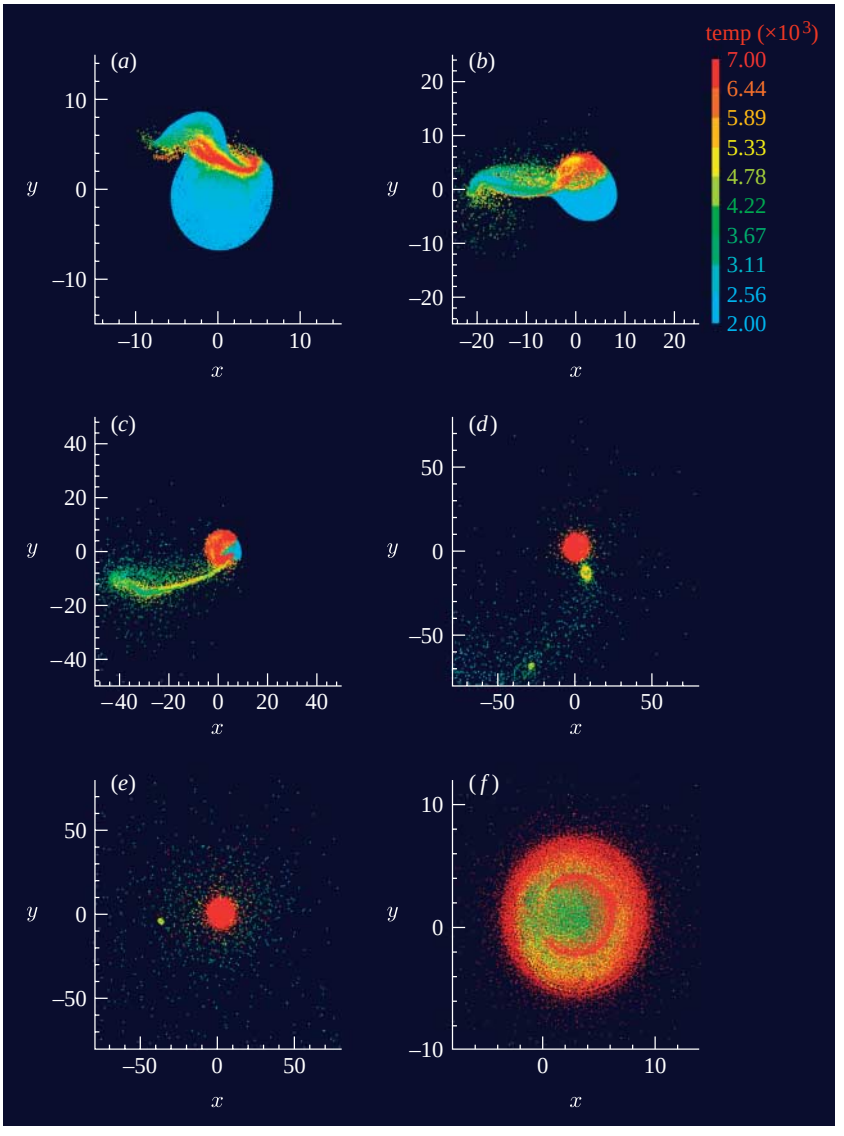

Figure 3. A potential lunar-forming impact (run 82 from Canup 2008) in which a $0.13M_{\oplus}$ impactor collides with a $0.89M_{\oplus}$ target with $b'=0.7$ ($\xi=45°$) and $(v_{\rm imp}/v_{\rm esc})=1.05$ (or $v_{\infty}\approx 3\ {\rm km\ s^{-1}}$). Both objects are differentiated and contain 70 per cent forsterite and 30 per cent iron by mass, described by the M-ANEOS equation of state (Melosh 2007). Prior to the collision, the target has a retrograde (i.e. in the opposite rotational sense as the impact) spin about the $\hat{z}$ axis with a period of 18 h. (*a–e*) Snapshots at progressive times looking down on the plane of the impact, with distances shown in units of 10^3 km (note the changes in scale between different frames). Colour scales with particle temperature in kelvin, with red particles having $T>6440$ K. (*a*) $t=0.32$ h, (*b*) $t=0.86$ h, (*c*) $t=2.2$ h, (*d*) $t=10.3$ h, and (*e*) $t=31.3$ h. (*e*) The final bound planet–disc system has an angular momentum equal to that of the current Earth–Moon system and contains $1.01M_{\oplus}$ after accounting for escaping material. (*f*) A close-up of the final thermal state of the planet. The partial red ring of high temperature material in the planet's interior is iron from the impactor's core that has accreted onto the Earth's core.

(*b*) *Properties of lunar-forming impacts*

Figure 3 shows an example SPH simulation of a potential Moon-forming impact (Canup 2008). In the hour following an oblique, low-velocity (i.e. $(v_{\rm imp}/v_{\rm esc})\sim 1$) collision, the impactor material that has grazed past the target initially forms an elongated structure that is nearly in line with its original trajectory (figure 3*b*). As this material undergoes Keplerian motion, it is 'wound up' into a structure coarsely resembling a trailing spiral arm (figure 3*c*). Gravitational torques across this structure allow outer portions to gain angular momentum and achieve orbit at the expense of inner portions, which recollide with the Earth. The inner portions of the arm (which consist primarily of the impactor's iron core) often recoalesce into a large clump (figure 3*d*) that re-impacts the planet, removing most of the impactor's iron from orbit. In this case, the orbiting disc (figure 3*e*) contains $1.4M_{\rm L}$, and is composed of 7 per cent iron and 85 per cent impactor material by mass. Of the orbiting particles, 50 per cent have orbital periapses outside the Earth's Roche limit.

The final disc in figure 3 contains an approximately $0.5M_{\rm L}$ intact clump that would probably be the lunar precursor. In most cases, the analogue to this clump has its periapsis within the Roche limit so that it is tidally disrupted within the first 20 hours or so after the initial impact. *N*-body simulations of the subsequent accretion of the Moon find that discs with or without large initial clumps typically produce a single satellite just outside the Roche limit in less than a year (e.g. Kokubo *et al.* 2000). However, such models may greatly underestimate the lunar accretion time scale because they neglect the disc's thermal evolution (e.g. Canup 2004*b*).

The Moon-forming impact delivers prodigious energy to the Earth, with $E_{\rm imp}/M_{\oplus}\sim 5\times 10^{10}\,{\rm erg\,g^{-1}}\,(\gamma/0.1)(v_{\rm imp}/10\,{\rm km\,s^{-1}})^2$, which is much greater than the latent heat of fusion for rock, $l\sim$few$\times 10^9\,{\rm erg\,g^{-1}}$. Figure 4 shows the initial and final temperatures within the target proto-Earth from the simulation in figure 3. The initial temperatures were generated by applying an adiabat with a 2000 K surface temperature to the uncompressed proto-Earth, which was subsequently settled with SPH to achieve a compressed hydrostatic state (as in the 'warm start' cases in Canup 2004*a*). Even when the target's interior is initially subsolidus, most of the proto-Earth is heated to a mixed solid–melt state, with material in the outer approximately 10^3 km of the proto-Earth melted completely. Extrapolation of the characteristic temperature increases in figure 4 to a more realistic starting condition of a proto-Earth at or above the solidus before the Moon-forming impact (e.g. Pritchard & Stevenson 2000) implies extensive complete melting throughout the Earth's mantle.

General trends in impact outcome as a function of b', $(v_{\rm imp}/v_{\rm esc})$ and γ have been observed (e.g. Canup & Asphaug 2001; Canup 2004*a*). For oblique, high-velocity impacts (with $b'>0.7$ and $(v_{\rm imp}/v_{\rm esc})\geq 1.2$), most of the impactor escapes and little mass is left in an orbiting disc. For low-velocity impacts (i.e. $(v_{\rm imp}/v_{\rm esc})\leq 1.1$), the disc mass generally increases as b' is increased, because increasing b' leads to a greater fraction of the impactor grazing past the target where it can most effectively be torqued into bound orbit. While collisions with $b'>0.75$ produce massive discs, they are too iron rich to yield the Moon. For a fixed b' and $(v_{\rm imp}/v_{\rm esc})$, increasing the impactor mass fraction γ typically increases the final disc mass.

Figure 5 shows results of impacts between rotating (Canup 2008) and non-rotating (Canup 2004*a*) objects that produced discs containing less than 10 per cent iron by mass. With or without pre-impact rotation, successful lunar-forming cases require $(v_{\rm imp}/v_{\rm esc}) \leq 1.1$ and $0.65 < b' < 0.75$. Cases that produce sufficiently massive discs to yield the Moon have discs that are derived primarily (60–90%) from the impactor's mantle (figure 5*b*). A target proto-Earth with a pre-impact retrograde rotation (i.e. in the opposite rotational sense to the impact itself; figure 5, red circles) allows for somewhat larger impactors (up to approx. $0.2M_{\oplus}$) and provides an improved match with the Earth–Moon system's angular momentum compared to the non-rotating cases (figure 5, black circles). A prograde rotating target (figure 5, blue circles) results in discs that are not massive enough in nearly all cases with $L_{\rm col} \sim L_{\rm EM}$. An impact-formed Moon argues against the Earth having had a low-obliquity, rapid prograde rotation before the lunar-forming event.

(*c*) *Implications and open issues*

A successful lunar-forming impact—defined as one that produces a sufficiently massive and iron-depleted disc to yield the Moon, a final planet mass of approximately $M_{\oplus}$, and a final system angular momentum of approximately $L_{\rm EM}$—requires (i) a differentiated impactor containing between $0.11M_{\oplus}$ and $0.2M_{\oplus}$, (ii) a relatively low-velocity impact, with $v_{\infty} < 4\,{\rm km\,s^{-1}}$, and (iii) an impact angle approximately between 40° and 50°. The giant impactor mass is similar to those expected for late stage oligarchs, and the impact velocity upper limit is comparable to the median encounter velocities of embryo–embryo collisions seen in accretion simulations (O'Brien *et al.* 2006). Because 45° is the most probable impact angle for randomly oriented impacts, approximately 15 per cent of all collisions would have $40^{\circ} \leq \xi \leq 50^{\circ}$.

An impactor origin of the majority of proto-lunar material is a universal prediction of all successful impact simulations, and one that must ultimately be reconciled with the identical O-isotope compositions of the Earth and the Moon (e.g. Wiechert *et al.* 2001). This appears to require either that the impactor and proto-Earth had identical compositions (unlikely, given the compositional variation predicted by accretion models) or that extensive mixing between proto-lunar and proto-Earth material after the impact but prior to the Moon's formation allowed compositions to equilibrate (Pahlevan & Stevenson 2007). The mixing scenario seems the most promising, but requires the Moon's formation to be delayed by a hundred years or more after the impact. Improved models of proto-lunar disc evolution and lunar accretion will be needed to assess whether this is plausible.

3. Summary

Terrestrial accretion dynamics is a mature field whose fundamentals are well developed and understood. However, some key effects have yet to be fully incorporated into the most recent models, including fragmentation, density-wave damping and type I migration. Of particular importance is the potential for substantial radial migration and loss of terrestrial proto-planets to collision with

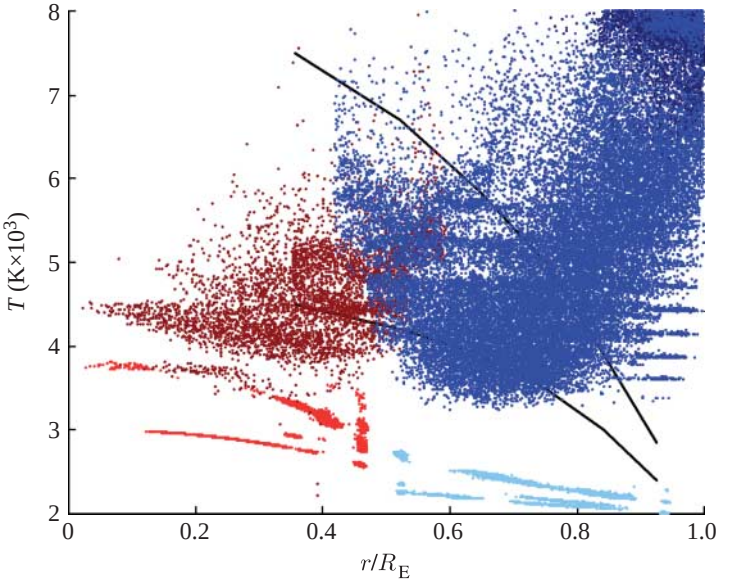

Figure 4. Temperature in the proto-Earth as a function of depth (where r is the distance from the planet's centre and $R_E = 6378$ km) for the impact simulation shown in figure 3. Iron and silicate particles in the initial, pre-impact proto-Earth are shown as red and light blue points. Dark red and blue points show the original proto-Earth material at the simulation's final time step (31 h), while dark blue points (upper right) are silicate particles originating from the impactor that are accreted by the proto-Earth. The great majority of the impactor's iron core is accreted by the proto-Earth, and this material has extremely high predicted post-impact temperatures (greater than 15 000 K) that are above the scale of this plot. Shown in black are example solidus and liquidus curves for a three-component ($MgSiO_3$, MgO and FeO) lower mantle magma ocean model (Solomatov & Stevenson 1993).

the Sun, which appears probable for nominal migration rates and nebular lifetimes. Migration would weaken the link between the planetary objects we see today and the original provenance of the material that comprises them.

That the final phase in the growth of terrestrial planets was dominated by giant impacts has become well accepted in the decades since its first demonstration (Wetherill 1985). As the last major event in the Earth's accretion, the Moon-forming impact is dynamically a relatively well-constrained problem. Successful simulations that can reproduce the current Earth–Moon system invoke impactor sizes and velocities predicted to be common during late stage terrestrial accretion. Models of the subsequent formation of the Moon from the proto-lunar disc are less well developed, and further work is needed to describe the coupled thermal and dynamical evolution of the disc and the Moon's initial thermal state. This should enable improved quantitative compositional and geophysical predictions for an impact-formed Moon, and its expected similarities and dissimilarities with the Earth.

I thank William Ward, Amy Barr and the reviewers for their helpful comments, and Scott Kenyon, Douglas McNeil and David O'Brien for providing me with figures from their publications. This work was supported by NASA's *Origins of Solar Systems Program*.

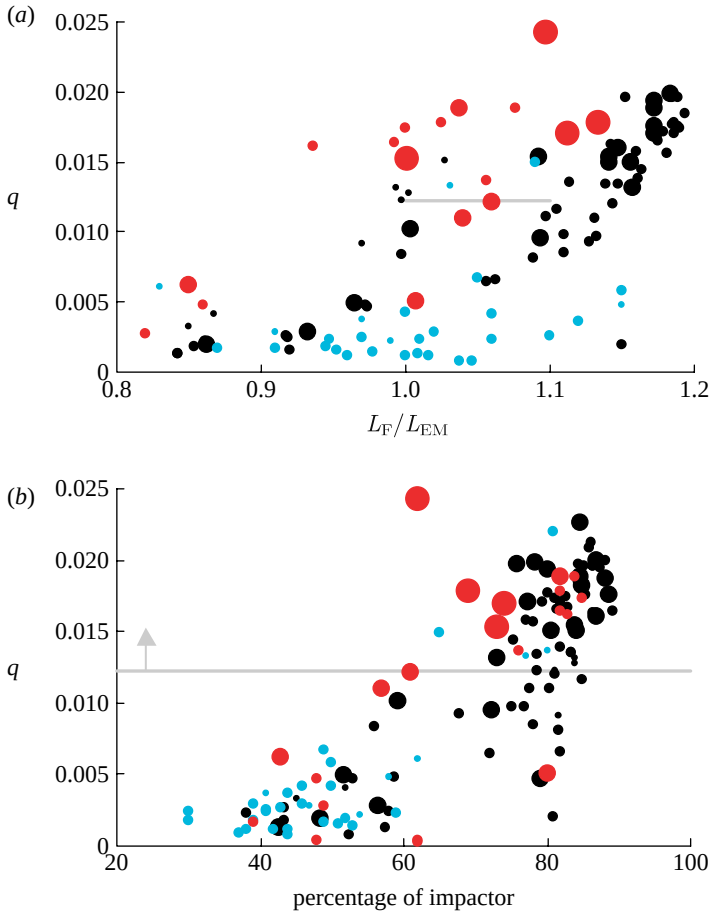

Figure 5. Results from SPH impact simulations that produced iron-depleted discs containing less than 10 per cent iron by mass (from Canup 2004*a*, 2008). Colour indicates pre-impact rotation state (red, retrograde target; black, no pre-impact spin; blue, prograde target), while symbol size scales with impactor size (small, $\gamma=0.11$; medium, $\gamma=0.13$; large, $\gamma=0.15$; extra large $\gamma=0.20$). (*a*) Predicted maximum satellite-to-planet mass ratio q, assuming no mass escapes from the proto-lunar disc (Ida *et al.* 1997) versus the final angular momentum of the bound planet–disc system L_F, in units of the Earth–Moon system's angular momentum L_{EM}. The current Earth–Moon system is indicated by the pale grey line (with $1 \leq L_F/L_{EM} \leq 1.1$ shown to allow for up to 10 per cent angular momentum loss over the system's history due to solar interactions). The largest q value shown reflects a disc mass of $2.1 M_L$ produced by the rather extreme case of an impact into a rapidly retrograde rotating target with a 4.1 h period prior to the lunar-forming collision. (*b*) Predicted maximum satellite-to-planet mass ratio versus the fraction of the disc mass that originates from the impactor.

References

Agnor, C. B. & Ward, W. R. 2000 Damping of terrestrial-planet eccentricities by density-wave interactions with a remnant gas disk. *Astrophys. J.* **567**, 579–586. (doi:10.1086/338415)

Agnor, C. B., Canup, R. M. & Levison, H. F. 1999 On the character and consequences of large impacts in the late stage of terrestrial planet formation. *Icarus* **142**, 219–237. (doi:10.1006/icar.1999.6201)

Benz, W., Cameron, A. G. W. & Melosh, H. J. 1989 The origin of the Moon and the single impact hypothesis III. *Icarus* **81**, 113–131. (doi:10.1016/0019-1035(89)90129-2)

Cameron, A. G. W. & Ward, W. R. 1976 The origin of the Moon. In *Proc. 7th Lunar and Planetary Science Conf., Lunar and Planetary Institute, Houston, Tx*, pp. 120–122.

Canup, R. M. 2004*a* Simulations of a late lunar forming impact. *Icarus* **168**, 433–456. (doi:10.1016/j.icarus.2003.09.028)

Canup, R. M. 2004*b* Dynamics of lunar formation. *Annu. Rev. Astron. Astrophys.* **42**, 441–475. (doi:10.1146/annurev.astro.41.082201.113457)

Canup, R. M. 2008 Lunar-forming collisions with pre-impact rotation. *Icarus* **196**, 518–538. (doi:10.1016/j.icarus.2008.03.011)

Canup, R. M. & Asphaug, E. 2001 Origin of the Moon in a giant impact near the end of the Earth's formation. *Nature* **412**, 708–712. (doi:10.1038/35089010)

Chambers, J. E. 2001 Making more terrestrial planets. *Icarus* **152**, 205–224. (doi:10.1006/icar.2001.6639)

Chambers, J. E. & Wetherill, G. W. 1998 Making the terrestrial planets: *N*-body integrations of planetary embryos in three dimensions. *Icarus* **136**, 304–327. (doi:10.1006/icar.1998.6007)

Goldreich, P., Lithwick, Y. & Sari, R. 2004 Planet formation by coagulation: a focus on Uranus and Neptune. *Annu. Rev. Astron. Astrophys.* **42**, 549–601. (doi:10.1146/annurev.astro.42.053102.134004)

Haisch Jr, K. E., Lada, E. A. & Lada, C. J. 2001 Disk frequencies and lifetimes in young clusters. *Astrophys. J.* **553**, L153–L156. (doi:10.1086/320685)

Halliday, A. N. & Kleine, T. 2006 Meteorites and the timing, mechanisms, and conditions of terrestrial planet accretion and early differentiation. In *Meteorites and the early Solar System II* (eds D. S. Lauretta & H. Y. McSween Jr), pp. 775–801. Tucson, AZ: University of Arizona Press.

Hartmann, W. K. & Davis, D. R. 1975 Satellite-sized planetesimals and lunar origin. *Icarus* **24**, 504–515. (doi:10.1016/0019-1035(75)90070-6)

Hayashi, C., Nakazawa, K. & Nakagawa, Y. 1985 Formation of the solar system. In *Protostars and planets II*, pp. 1100–1153. Tucson, AZ: University of Arizona Press.

Hubickyj, O., Bodenheimer, P. & Lissauer, J. J. 2005 Accretion of the gaseous envelope of Jupiter around a 5–10 Earth-mass core. *Icarus* **179**, 415–431. (doi:10.1016/j.icarus.2005.06.021)

Ida, S., Canup, R. M. & Stewart, G. R. 1997 Lunar accretion from an impact generated disk. *Nature* **389**, 353–357. (doi:10.1038/38669)

Johansen, A., Oishi, J. S., Mac Low, M., Klahr, H., Henning, T. & Youdin, A. 2007 Rapid planetesimal formation in turbulent circumstellar disks. *Nature* **448**, 1022–1025. (doi:10.1038/nature06086)

Kenyon, S. J. & Bromley, B. C. 2006 Terrestrial planet formation I. The transition from oligarchic growth to chaotic growth. *Astron. J.* **131**, 1837–1850. (doi:10.1086/499807)

Kokubo, E. & Ida, S. 2002 Formation of protoplanet systems and diversity of planetary systems. *Astrophys. J.* **581**, 666–680. (doi:10.1086/344105)

Kokubo, E., Ida, S. & Makino, J. 2000 Evolution of a circumterrestrial disk and formation of a single Moon. *Icarus* **148**, 419–436. (doi:10.1006/icar.2000.6496)

Kokubo, E., Kominami, J. & Ida, S. 2006 Formation of terrestrial planets from protoplanets. I. Statistics of basic dynamical properties. *Astrophys. J.* **642**, 1131–1139. (doi:10.1086/501448)

McNeil, D., Duncan, M. & Levison, H. F. 2005 Effects of type I migration on terrestrial planet formation. *Astron. J.* **130**, 2884–2899. (doi:10.1086/497687)

Melosh, H. J. 2007 A hydrocode equation of state for SiO_2. *Meteorit. Planet. Sci.* **42**, 2079–2098.

Nagasawa, M., Lin, D. N. C. & Thommes, E. 2005 Dynamical shake-up of planetary systems. I. Embryo trapping and induced collisions by the sweeping secular resonance and embryo–disk tidal interaction. *Astrophys. J.* **635**, 578–598. (doi:10.1086/497386)

O'Brien, D. P., Morbidelli, A. & Levison, H. F. 2006 Terrestrial planet formation with strong dynamical friction. *Icarus* **184**, 39–58. (doi:10.1016/j.icarus.2006.04.005)

Paardekooper, S.-J. & Mellema, G. 2006 Halting type 1 planet migration in non-isothermal disks. *Astron. Astrophys.* **459**, L17–L20. (doi:10.1051/0004-6361:20066304)

Pahlevan, K. & Stevenson, D. J. 2007 Equilibration in the aftermath of the lunar-forming giant impact. *Earth Planet. Sci. Lett.* **262**, 438–449. (doi:10.1016/j.epsl.2007.07.055)

Pritchard, M. E. & Stevenson, D. J. 2000 Thermal aspects of a lunar origin by giant impact. In *Origin of the Earth and Moon* (eds R. M. Canup & K. Righter), pp. 179–196. Tucson, AZ: University of Arizona Press.

Rafikov, R. R. 2001 Termination of planetary accretion due to gap formation. *Astron. J.* **122**, 2713–2722. (doi:10.1086/323451)

Solomatov, V. S. & Stevenson, D. J. 1993 Nonfractional crystallization of a terrestrial magma ocean. *J. Geophys. Res.* **98**, 5391–5406. (doi:10.1029/92JE02579)

Tanaka, H., Takeuchi, T. & Ward, W. R. 2002 Three-dimensional interaction between a planet and an isothermal gaseous disk. I. Corotation and Lindblad torques and planet migration. *Astrophys. J.* **565**, 1257–1274. (doi:10.1086/324713)

Thommes, E. W., Duncan, M. J. & Levison, H. F. 2003 Oligarchic growth of giant planets. *Icarus* **161**, 431–455. (doi:10.1016/S0019-1035(02)00043-X)

Wada, K., Kokubo, E. & Makino, J. 2006 High-resolution simulations of a Moon-forming impact and postimpact evolution. *Astrophys. J.* **638**, 1180–1186. (doi:10.1086/499032)

Ward, W. R. 1986 Density waves in the solar nebula—differential Lindblad torque. *Icarus* **67**, 164–180. (doi:10.1016/0019-1035(86)90182-X)

Ward, W. R. 1998 On disk–planet interactions and orbital eccentricities. *Icarus* **73**, 330–348. (doi:10.1016/0019-1035(88)90103-0)

Ward, W. R. 2000 On planetesimal formation: the role of collective particle behavior. In *Origin of the Earth and Moon* (eds R. M. Canup & K. Righter), pp. 75–84. Tucson, AZ: University of Arizona Press.

Weidenschilling, S. J. & Cuzzi, J. N. 1993 Formation of planetesimals in the solar nebula. In *Protostars and planets III* (eds E. H. Levy & J. Lunine), pp. 1031–1060. Tucson, AZ: University of Arizona Press.

Weidenschilling, S. J., Spaute, D., Davis, D. R., Marzari, F. & Ohtsuki, K. 1997 Accretional evolution of a planetesimal swarm. *Icarus* **128**, 429–455. (doi:10.1006/icar.1997.5747)

Wetherill, G. W. 1985 Occurrence of giant impacts during the growth of terrestrial planets. *Science* **228**, 877–879. (doi:10.1126/science.228.4701.877)

Wiechert, U., Halliday, A. N., Lee, D.-C., Snyder, G. A., Taylor, l. A. & Rumble, D. 2001 Oxygen isotopes and the Moon-forming giant impact. *Science* **294**, 345–348. (doi:10.1126/science.1063037)